Polymer Chemistry

ROYAL SOCIETY OF CHEMISTRY

PAPER

View Article Online
View Journal | View Issue

Cite this: *Polym. Chem.*, 2024, **15**, 4231

A facile and versatile platform for preparing uniform π-conjugated nanofibers with controlled length and varying shells†

Bo Xiang,[a] Hongluo Wu,[a] Rang Chen,[a] Xiaoyu Huang, *[a,b] Guolin Lu[a] and Chun Feng*[a,c]

The development of facile, efficient and versatile approaches for preparing π-conjugated-polymer-based nanofibers (CPNFs) with controlled length, composition and surface chemistry is of paramount importance due to the promising applications of CPNFs in fields ranging from electronics to nanomedicine. In this article, we report the generation of uniform CPNFs consisting of a π-conjugated oligo(*p*-phenylenevinylene) (OPV_5) core and coronas of diverse properties with controllable length by the combination of activated-ester/amine chemistry and a self-seeding approach of living crystallization-driven self-assembly (CDSA). Poly(pentafluorophenyl methacrylate) (PPFMA) is used as a versatile precursor to efficiently prepare diverse corona-forming segments by "click-type" activated-ester/amine chemistry. Subsequently, amine-based 18-crown-ether-6 (18C6) and dimethylamino (DMA) groups used as model functional moieties were treated with the pentafluorophenyl esters of PPFMA, followed by coupling with OPV_5 to afford OPV_5-containing BCPs with varying corona-forming segments. By the self-seeding approach of living CDSA, uniform fiber-like micelles with either 18C6- or DMA-based coronas with controlled length can be obtained. The 18C6 and DMA units enable the installation of diverse functional units, such as metal ions, metal clusters, metal nanoparticles, chiral amines and porphyrins. This work presents a facile and versatile platform to generate uniform CPNFs with controlled length and varying functionalities.

Received 6th September 2024,
Accepted 24th September 2024

DOI: 10.1039/d4py00979g

rsc.li/polymers

Introduction

π-Conjugated-polymer-based nanofibers (CPNFs) endowed with merits of both one-dimensional (1-D) nanostructures, known for their high aspect ratio and specific surface area, and π-conjugated polymers, known as flexible semiconductors with tunable electronic/optical/magnetic properties, have promising applications in electronics, nanomedicine, catalysis and sensing.[1–4] It is well-documented that the length (dimension), composition, and surface chemistry of CPNFs are key factors in determining their properties.[5–10] Therefore, the development of facile, efficient and versatile approaches for preparing CPNFs with controlled length, composition and surface chemistry has attracted increasing interest.

Self-assembly of amphiphilic block copolymers (BCPs) with a core-forming π-conjugated segment mainly driven by the solvophobic effect has been widely used to generate CPNFs.[11,12] Owing to the unique morphology of fiber-like nanostructures, morphology-pure fiber-like micelles can only be formed under some strict experimental conditions and polymer compositions. Even if morphology-pure fiber-like micelles are formed, their length and composition are hard to control.[13,14] In recent decades, the self-assembly of coil-crystalline BCPs predominantly driven by the crystallization effect of core-forming crystalline segments, referred to as living crystallization-driven self-assembly (CDSA) including seeded growth and self-seeding approaches, has emerged. This strategy allows one to generate morphology-pure fiber-like nanostructures with precisely designed composition/dimension/morphology under optimized conditions.[15–19] Due to strong π–π stacking and charge transfer interactions within the π-conjugated units, the π-conjugated units with optimized structures/compositions also demonstrate crystallinity.[4,20–31] By taking advantage of the

[a]*Key Laboratory of Synthetic and Self-Assembly Chemistry for Organic Functional Molecules, Shanghai Institute of Organic Chemistry, University of Chinese Academy of Sciences, Chinese Academy of Sciences, 345 Lingling Road, Shanghai 200032, People's Republic of China. E-mail: cfeng@ecust.edu.cn; Tel: +86-21-54925606*
[b]*Macau University of Science and Technology, Faculty of Medicine, Macau SAR, 999078, China. E-mail: xyhuang@mail.sioc.ac.cn; Tel: +86-21-54925310*
[c]*Shanghai Key Laboratory of Advanced Polymeric Materials, School of Materials Science and Engineering, East China University of Science and Technology, 130 Meilong Road, Shanghai 200237, People's Republic of China*

†Electronic supplementary information (ESI) available: Polymer synthesis and characterization, procedures of sample preparation, TEM images of micelles, and characterization/analysis of micelles. See DOI: https://doi.org/10.1039/d4py00979g

crystallinity of π-conjugated polymers (oligomers), uniform CPNFs with controlled composition/length can be generated by self-seeding and seeded growth approaches of living CDSA from BCPs containing a crystalline π-conjugated segment.[22,23] The examples of crystalline π-conjugated blocks that have been used in the generation of uniform CPNFs include poly(fluorene) (PF),[8,24] poly(thiophene) (PT),[25–27] poly(selenophene) (PSe),[28] oligo(*p*-phenylenevinylene) (OPV),[29] oligo(*p*-phenylene ethynylene) (OPE)[30] and polyacetylene-derivatives.[31]

Previous studies revealed that the structure, including the chemical composition and chain length, of corona-forming segments was one of the most vital factors affecting CDSA behaviors (self-seeding and seeded growth processes). During the micellar evolution process in CDSA, some typical crystalline segments of poly(ferrocenyldimethylsilane) (PFS), poly(L-lactide), poly(ε-caprolactone) and polyethylene[23,32–34] usually fold to form crystals to minimize the steric repulsion within the corona-forming chains, whereas most of the π-conjugated polymers (oligomers) are hard to fold due to their backbone rigidity. In this context, the structures/properties of the corona-forming segments of π-conjugated-polymer-based BCPs exhibited much more pronounced influence on both the morphology of formed micelles and the kinetics of micellar evolution.[35–39] For example, He and co-workers systematically examined the self-assembly of PPV_7-*b*-$P2VP_n$ (PPV = poly(*p*-phenylenevinylene), P2VP = poly(2-vinylpyridine), n = 27 and 54) in methanol. It was found that PPV_7-*b*-$P2VP_{27}$ self-assembled to form scarf-like micelles, whereas PPV_7-*b*-$P2VP_{54}$ only formed fiber-like micelles under the same conditions due to enhanced steric repulsion within the P2VP chains.[35] Kinetic studies on the CDSA of OPV_5-*b*-$PNIPAM_{18}$ (PNIPAM = poly(*N*-isopropylacrylamide)), OPV_5-*b*-$PNIPAM_{49}$ and OPV_5-*b*-$PNIPAM_{75}$ revealed that only OPV_5-*b*-$PNIPAM_{49}$ followed a living micellar elongation process to give uniform fiber-like micelles with controlled length in the seeded growth process. Due to the much faster aggregation rate for OPV_5-*b*-$PNIPAM_{18}$ and higher steric repulsion within the $PNIPAM_{75}$ chains of OPV_5-*b*-$PNIPAM_{75}$, self-nucleation was prone to occur during the seeded growth process of these systems, which led to the formation of polydisperse fiber-like micelles.[37,38] Another report on the self-seeding of OPV_5-*b*-$PHPMA_{71}$ and OPV_5-*b*-$PHPMA_{100}$ (PHPMA = poly(*N*-(2-hydroxypropyl) methacrylamide)) showed that monodisperse fiber-like micelles with controlled length can be generated by self-seeding of OPV_5-*b*-$PHPMA_{71}$, whereas only polydisperse short fiber-like micelles with length below 100 nm were generated for OPV_5-*b*-$PHPMA_{100}$ under similar conditions as a consequence of the occurrence of self-nucleation/growth that was due to much more pronounced steric repulsion within the $PHPMA_{100}$ chains.[36] Therefore, one has to optimize the chain length and chemical composition of the corona-forming segments of crystalline-coil block copolymers to generate uniform CPNFs with controlled composition/length by living CDSA.

To create CPNFs with diverse functionalities, one efficient and facile approach is to vary the properties, that is, the chemical structure/composition, of corona-forming segments. For instance, for CPNFs containing an OPE_9 core, as the corona-forming segment of PNIPAM was replaced by poly(polypropyl-3-methanethiol acrylate) (PMTPA), of which methylthio groups can coordinate with metal nanoparticles/ions and undergo click-type nucleophilic substitution to give positively charged sulfonium groups, multi-functional CPNFs with catalytic and antibacterial activities can be obtained.[40] Although the above two kinds of CPNFs contained the same core-forming segment of OPE_9, separate polymerization reactions were conducted to obtain targeted corona-forming PNIPAM and PMTPA chains, respectively. Since the monomers with different structures usually have distinct polymerization reactivities, as one would like to prepare different corona-forming polymers, one usually has to devote significant efforts to the optimization of polymerization conditions case by case to obtain targeted corona-forming polymers with designed chain lengths.[4,20,41] This routine way towards the synthesis of corona-forming chains is tedious, and thus the development of more facile and versatile approaches for the preparation of corona-forming chains with diverse properties/functionalities for π-conjugated-polymer-based BCPs is highly desired.

The pentafluorophenyl ester exhibits attractive activated-ester/amine chemistry that shows high reactivity and wide functional-group tolerance toward amines for introducing diverse functional groups under mild reaction conditions.[42–44] Thus, the pentafluorophenyl ester chemistry has been employed in postpolymerization modification to prepare various functional polymers.[45] Inspired by these results, herein, we report a facile and efficient platform to create uniform CPNFs containing an OPV_5 core and 18-crown-ether-6- (18C6) or dimethylamino (DMA)-based coronas by the combination of pentafluorophenyl ester chemistry and the self-seeding approach of living CDSA, in which poly(pentafluorophenyl methacrylate) (PPFMA) is used as the same precursor to prepare corona-forming segments of diverse structures (Scheme 1). Subsequently, the resulting corona-forming segments are coupled with OPV_5 to give OPV_5-based BCPs with varying corona-forming segments. The self-seeding of the resulting OPV_5-containing BCPs affords monodisperse fiber-like micelles with controlled length. By virtue of the coordinating capacities of 18C6 and DMA groups of the resulting coronas, extra functional groups, including metal ions, metal clusters, metal nanoparticles and porphyrins, can be incorporated into the coronas of formed micelles to afford CPNFs with tunable structures/functionalities.

Results and discussion

Synthesis of OPV_5-containing block copolymers

The pentafluorophenyl ester exhibits attractive activated-ester chemistry that shows high reactivity and wide functional-group tolerance toward amines for *trans*-esterification under mild reaction conditions, and thus the pentafluorophenyl ester chemistry has been widely employed in the synthesis of polymers with varying functional groups.[42–44] In this context,

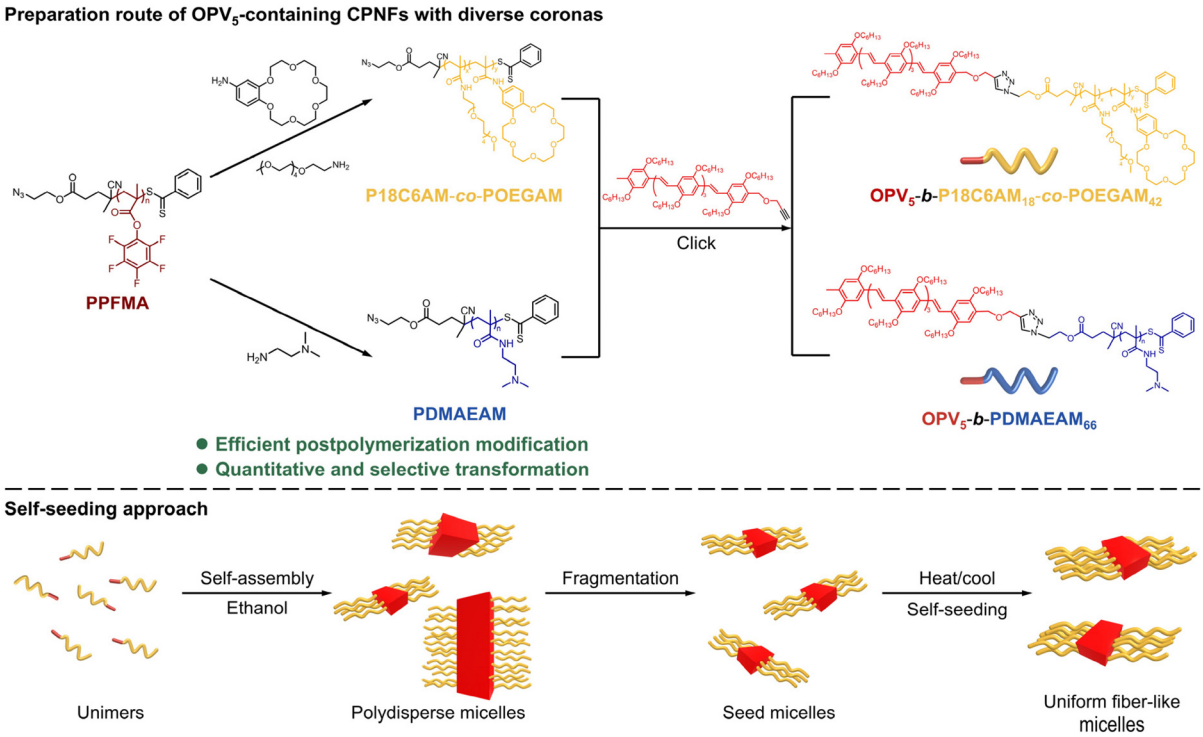

Scheme 1 Preparation route of OPV_5-containing CPNFs with controlled length and varying coronas by the combination of pentafluorophenyl ester chemistry and the self-seeding approach of living CDSA.

we first prepared azide-terminated poly(pentafluorophenyl methacrylate) (PPFMA) by reversible addition–fragmentation chain transfer (RAFT) polymerization with an azide-containing chain transfer agent according to previous reports.[42–44] Typical peaks at −150.64, −156.59 and −161.80 ppm attributed to the fluorine of the pentafluorophenyl unit and peaks at 2.44 and 1.39 ppm originating from the protons of the methacrylate segment appeared in the ^{19}F NMR and ^{1}H spectra of the obtained PPFMA (Fig. 1A and S1†), respectively. GPC analysis indicates a unimodal peak with a polydispersity of 1.13 (Fig. S2†). These results verify the structure of targeted PPFMA.

Subsequently, we attempted to introduce 18-crown-ether-6 (18C6) into PPFMA to give PPFMA-*co*-P18C6AM by treating PPFMA with amine-containing 18C6 with [18C6]:[PFMA] = 3 : 10 for 48 h. From the *in situ* ^{19}F NMR spectrum of the reaction mixture (Fig. 1B), typical peaks 'f', 'e' and 'g' at −169.67, −172.32 and −188.88 ppm attributed to the fluorine of pentafluorophenol appeared with the persistence of peaks 'b', 'c' and 'a' at −152.52, −159.80 and −164.65 ppm originating from the fluorine of the pentafluorophenyl units of PPFMA, indicative of partial *trans*-esterification to install 18C6 moieties.

The obtained sample with the introduced 18C6 units was further treated with 2,5,8,11,14-pentaoxahexadecan-16-amine (OEG) to install OEG side chains to give P18C6AM-*co*-POEGAM. After 5 h, the *in situ* ^{19}F NMR analysis revealed that typical peaks attributed to the fluorine of the pentafluorophenyl units of PPFMA completely disappeared with the appearance of peaks attributed to the fluorine of pentafluorophenol (Fig. 1C), which indicated that all of the remaining pentafluorophenyl units reacted with 2,5,8,11,14-pentaoxahexadecan-16-amine. The installation of OEG was further verified by the appearance of peaks at 3.32 ppm attributed to the –OCH_3 of OEG units, with the persistence of characteristic peaks at 4.02 to 3.60 ppm attributed to the –OCH_2CH_2O– of 18C6 units (Fig. 1D). Additionally, GPC analysis indicated a unimodal peak with a polydispersity of 1.15, comparable to that of pristine PPFMA (Fig. S3†). All the above results showed that both 18C6 and OEG groups can be introduced to PPFMA efficiently to give azide-terminated P18C6AM-*co*-POEGAM without inducing chain degradation or cross-linking.

We then synthesized alkyne-terminated OPV_5, which was used as a model π-conjugated block for the preparation of π-conjugated-polymer-based BCPs with varying corona-forming segments, according to our previous report[37] (the details about the synthesis and characterization of alkyne-terminated OPV_5 are provided in ESI Fig. S5–7†). The alkyne-terminated OPV_5 and azide-terminated P18C6AM-*co*-POEGAM were linked by the copper-catalyzed alkyne–azide cycloaddition (CuAAC) reaction. After removal of unreacted OPV_5 and P18C6AM-*co*-POEGAM by repeated precipitation in *n*-hexane and dialysis against ethanol (molecular weight cut-off: 50 000 g mol^{-1}), the purified sample was subjected to ^{1}H NMR and GPC analyses (Fig. 1 and S7†). A unimodal peak appeared in the GPC curve of the resulting OPV_5-*b*-P18C6AM-*co*-POEGAM (Fig. S7†), indicative of the complete removal of OPV_5 and P18C6AM-*co*-POEGAM. One can note typical peaks at 4.04 ppm attributed to

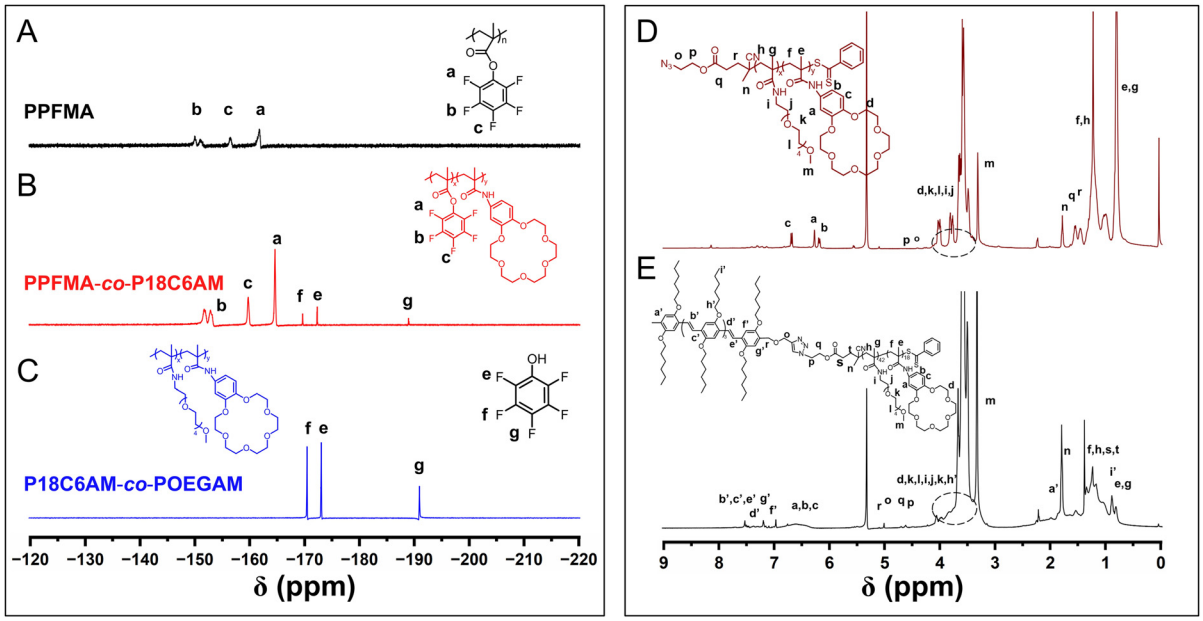

Fig. 1 (A) ^{19}F NMR spectra of azide-terminated PPFMA. ^{19}F NMR spectra of amidation reaction solutions of PPFMA-*co*-P18C6AM (B) and P18C6AM-*co*-POEGAM (C). ^{1}H NMR spectra of azide-terminated P18C6AM-*co*-POEGAM (D) and OPV_5-*b*-P18C6AM-*co*-POEGAM (E) (CD_2Cl_2).

the alkyl side chains ($-OC_6H_{13}$) of OPV_5, peaks at 3.56 ppm that originated from the protons of 18C6 and peak 'm' at 3.31 ppm attributed to the protons of OEG side chains (Fig. 1E). On the basis of ^{1}H NMR results and the known molecular weight of the OPV_5 segment, the number of 18C6 and OEG repeat units was estimated to be about 18 and 42, respectively. All the above results indicated that OPV_5-*b*-$P18C6AM_{18}$-*co*-$POEGAM_{42}$ with tunable composition can be efficiently prepared by the combination of pentafluorophenyl ester chemistry, CuAAC and RAFT polymerization.

CDSA of OPV_5-*b*-$P18C6AM_{18}$-*co*-$POEGAM_{42}$

Polydisperse fiber-like micelles by a direct heating–cooling protocol. Given the crystallinity of the OPV_5 segment, we then examined the CDSA of OPV_5-*b*-$P18C6AM_{18}$-*co*-$POEGAM_{42}$. An aliquot of OPV_5-*b*-$P18C6AM_{18}$-*co*-$POEGAM_{42}$ in ethanol (0.05 mg mL^{-1}) was subjected to heating at 80 °C for 30 min and then allowed to cool and age at 25 °C for 24 h (heating–cooling protocol, Fig. 2A). The TEM image showed that fiber-like micelles with a width of 16 nm and lengths up to several micrometers were formed (Fig. 2B and C). From the UV/vis absorption spectra of OPV_5-*b*-$P18C6AM_{18}$-*co*-$POEGAM_{42}$ in THF (Fig. 2D), a good solvent for both OPV_5 and $P18C6AM_{18}$-*co*-$POEGAM_{42}$ segments, and the obtained micellar solution, one can note that the micellar solution exhibited about a 33 nm blue-shift compared to that in THF. In addition, about a 20 nm blue-shift with about 37% decrease in fluorescence intensity was also observed for the micellar solution in comparison with that of the THF solution (Fig. 2E). These results indicated that OPV_5 segments seemingly adopt a face-to-face H-aggregate mode to form the core of micelles, which was consistent with our previous reports.[29,37,45]

Self-seeding of OPV_5-*b*-$P18C6AM_{18}$-*co*-$POEGAM_{42}$ with Na^+ and K^+ ions. Self-seeding has been considered a facile approach for generating uniform micelles with length dispersity below ~1.3 by varying annealing temperatures.[29,30] To proceed, the as-prepared fiber-like micelles of OPV_5-*b*-$P18C6AM_{18}$-*co*-$POEGAM_{42}$ were fragmented with mild sonication (SONICS VC 750 ultrasonic processor, 50% power) at 0 °C for 30 min to obtain short fiber-like micelles (seeds, L_n = 55 nm, L_w/L_n = 1.13, L_n and L_w are number- and weight-average length of micelles, Fig. 3A). Subsequently, aliquots of seed micelles obtained from the same batch (0.05 mg mL^{-1} in ethanol) were heated at different temperatures (40 °C, 45 °C, 50 °C, 55 °C and 60 °C) for 30 min, followed by cooling/aging at 25 °C for 24 h. TEM analysis showed that uniform fiber-like micelles (L_w/L_n < 1.20) were obtained (Fig. 3B–D and S8, Table S1†). As the temperature increased from 45 °C to 50 °C, the L_n of the obtained micelles increased from 176 nm to 321 nm (Fig. 3B and S8, Table S1†). As the temperature increased to 65 °C, the L_n of the micelles sharply increased to 2387 nm (Fig. S8 and Table S1†). On the basis of the length of the initial seeds ($L_{n,0}$) and the obtained micelles at different temperatures ($L_{n,T}$), the fraction of survived seeds (P_T) can be estimated using the equation $P_T = L_{n,0}/L_{n,T}$, assuming that neither self-nucleation nor micellar coupling occurred during the whole self-seeding process.[29,37,45] The P_T was plotted against the annealing temperature (Fig. 3F). One can note that P_T decreased exponentially with the temperature, which is a key characteristic of the self-seeding process.[29,30] These results indicated that the self-seeding of OPV_5-*b*-$P18C6AM_{18}$-*co*-$POEGAM_{42}$ followed a controlled process.

Given the high coordinating capacity of crown-ether, especially 18C6 of OPV_5-*b*-$P18C6AM_{18}$-*co*-$POEGAM_{42}$, with

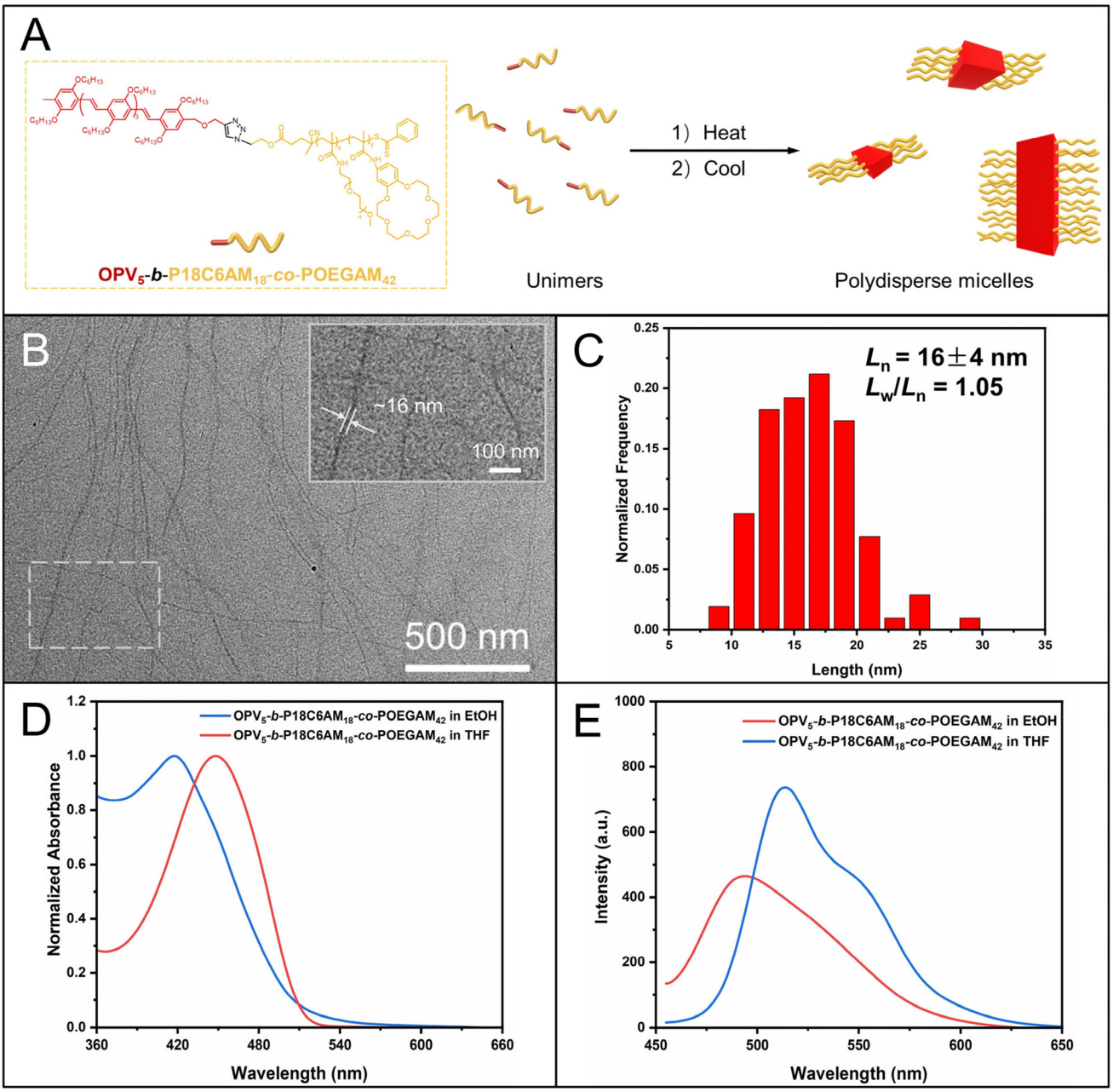

Fig. 2 (A) Schematic illustration of the formation of uniform fiber-like micelles of OPV_5-*b*-P18C6AM$_{18}$-*co*-POEGAM$_{42}$ by the self-seeding approach of living CDSA. (B) TEM image and (C) width distribution histogram of fiber-like micelles of OPV_5-*b*-P18C6AM$_{18}$-*co*-POEGAM$_{42}$ (0.05 mg mL^{-1} in ethanol). (D) UV/vis absorption and (E) fluorescence spectra of OPV_5-*b*-P18C6AM$_{18}$-*co*-POEGAM$_{42}$ in ethanol (0.05 mg mL^{-1}) and THF (0.05 mg mL^{-1}).

alkali metal ions such as Na^+ and K^+ with a complex constant (logK) of 4.13 and 6.05 in ethanol,[46,47] respectively, the 18C6-containing corona chains of fiber-like micelles could be used to introduce these alkali metal ions. We then examined the influence of complexation of 18C6 with these alkali metal ions on self-seeding behavior. Aliquots of seed solution were incubated with CH_3COONa and CH_3COOK, respectively, with a molar ratio of the 18C6 unit to metal ions of 1 : 1 and then subjected to a self-seeding protocol similar to that described for OPV_5-*b*-P18C6AM$_{18}$-*co*-POEGAM$_{42}$.

Firstly, when the annealing temperatures increased from 45 °C to 65 °C, uniform fiber-like micelles (L_w/L_n < 1.25) were obtained (Fig. 4B–D and S9 and S10, Tables S2 and S3†), regardless of the presence of CH_3COONa and CH_3COOK. Additionally, for these two sets of samples, P_T decreased exponentially with the temperature (Fig. 4F and S9 and S10, Tables S2 and S3†). These results indicated a controlled fashion of self-seeding in the presence of CH_3COONa and CH_3COOK. Secondly, the L_n of the formed micelles in the presence of CH_3COONa and CH_3COOK was lower than that of micelles

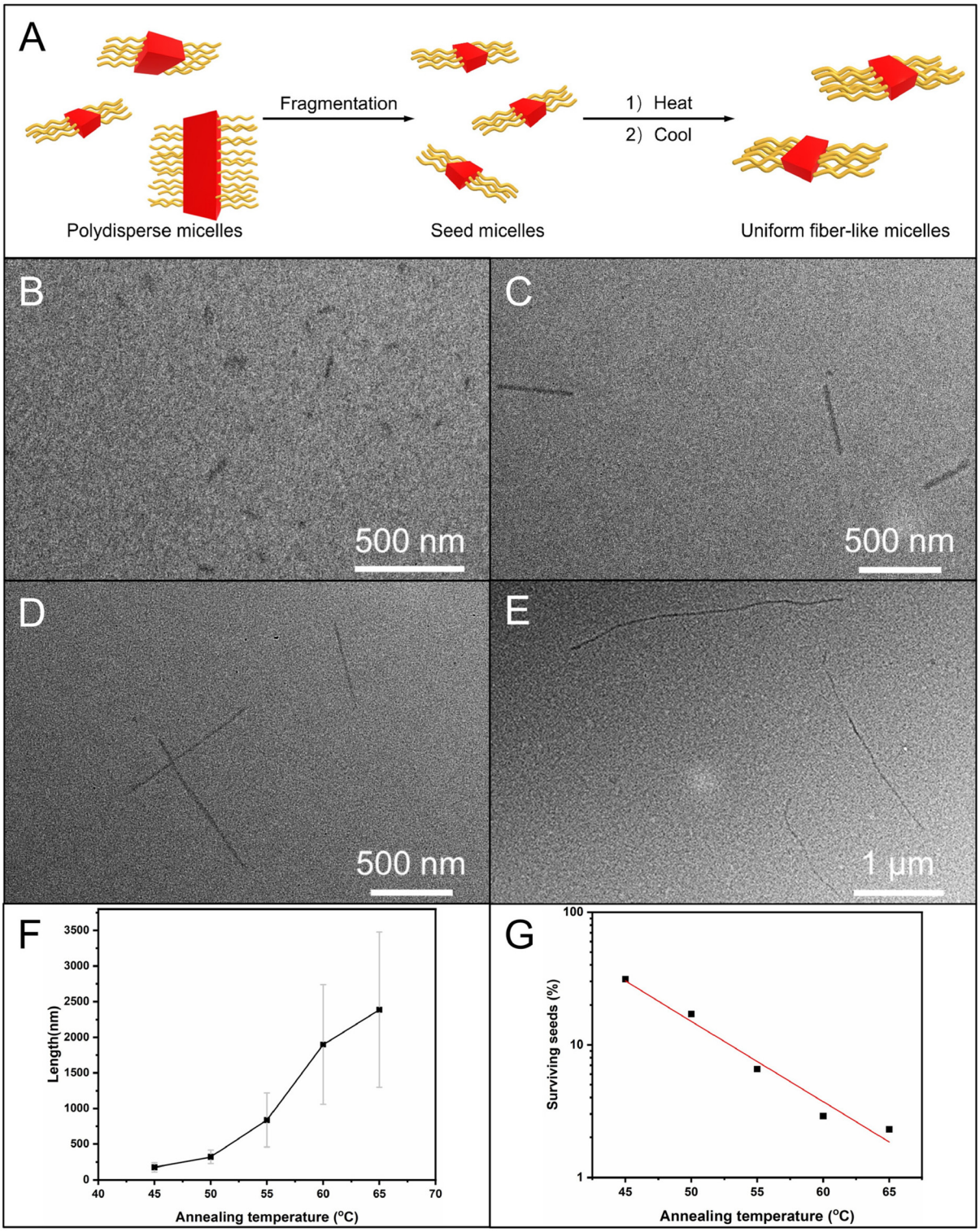

Fig. 3 (A) Schematic illustration of the formation of uniform fiber-like micelles of OPV_5-*b*-P18C6AM$_{18}$-*co*-POEGAM$_{42}$ by the self-seeding approach of living CDSA. TEM images of (B) seed micelles, and micelles formed by the self-seeding of OPV_5-*b*-P18C6AM$_{18}$-*co*-POEGAM$_{42}$ at annealing temperatures of (C) 50 °C, (D) 55 °C and (E) 60 °C. Dependence of (F) L_n of micelles formed by the self-seeding of OPV_5-*b*-P18C6AM$_{18}$-*co*-POEGAM$_{42}$ micelles and (G) percentages of surviving seeds on annealing temperature.

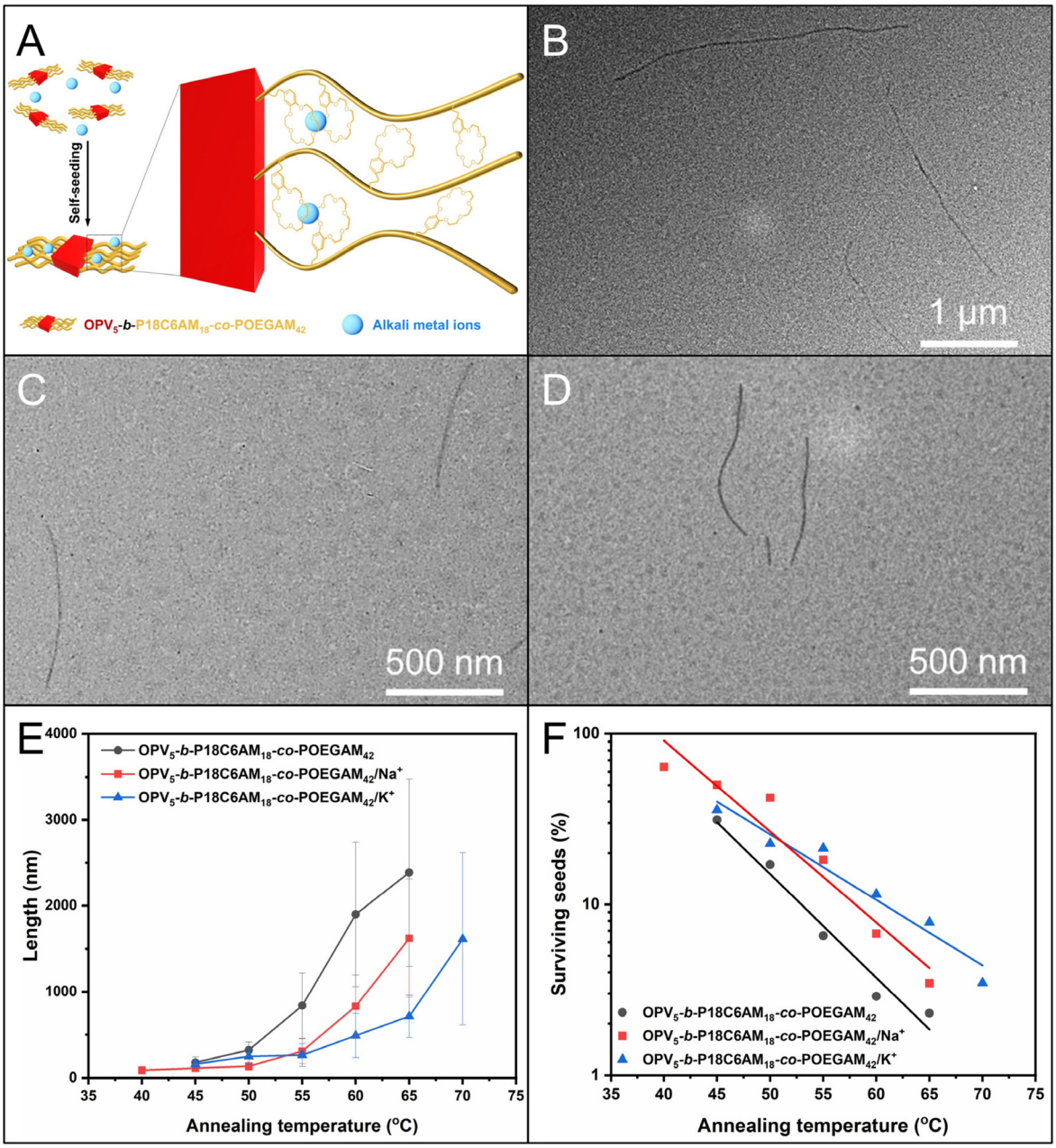

Fig. 4 (A) Schematic illustration of the self-seeding of OPV_5-*b*-$P18C6AM_{18}$-*co*-$POEGAM_{42}$ with alkali metal ions Na^+ and K^+. Typical TEM images of the fiber-like micelles of OPV_5-*b*-$P18C6AM_{18}$-*co*-$POEGAM_{42}$ by the self-seeding approach at an annealing temperature of 60 °C (B) without and with (C) CH_3COONa and (D) CH_3COOK, respectively. (E) L_n of fiber-like micelles and (F) semilogarithmic plot of the fraction of surviving seeds of OPV_5-*b*-$P18C6AM_{18}$-*co*-$POEGAM_{42}$ *versus* annealing temperature (0.05 mg mL^{-1} in ethanol) with and without CH_3COONa and CH_3COOK.

without these salts at the same temperature (Fig. 4E and S8–10, Tables S2 and S3†). Moreover, the fraction of surviving seeds without CH_3COONa and CH_3COOK was also lower than that with CH_3COONa and CH_3COOK at each temperature (Fig. 4F and S8–10, Tables S2 and S3†). This phenomenon indicated that the seeds in the presence of CH_3COONa and CH_3COOK had much higher resistance toward dissolution upon annealing. Thirdly, the L_n of micelles with the addition of CH_3COOK was comparable to that with the addition of CH_3COONa at the temperature from 45 °C to 55 °C, but became much lower at temperatures of 60 °C and 65 °C (Fig. 4E and S9 and S10, Tables S2 and S3†). The observations might reveal that the different self-seeding behavior should be mainly due to the alkali metal ions Na^+ and K^+, not the counter ion of CH_3COO^-. Furthermore, the enhancement of resistance of seed micelles in the presence of CH_3COONa and CH_3COOK indicated that the complexation of 18C6 with Na^+ and K^+ ions indeed occurred over the self-seeding process

(Fig. 4A). Additionally, the peaks attributed to 18C6 units showed a down-field shift in the presence of Na^+ and K^+ ions, which also demonstrated the complexation of 18C6 units with Na^+ and K^+ ions (Fig. S11†). This notion is further supported by a more noticeable blue-shift for OPV_5-*b*-$P18C6AM_{18}$-*co*-$POEGAM_{42}$ (0.05 mg mL^{-1} in ethanol) in the presence of CH_3COOK in temperature-dependent UV/vis absorption spectra (Fig. S12†).

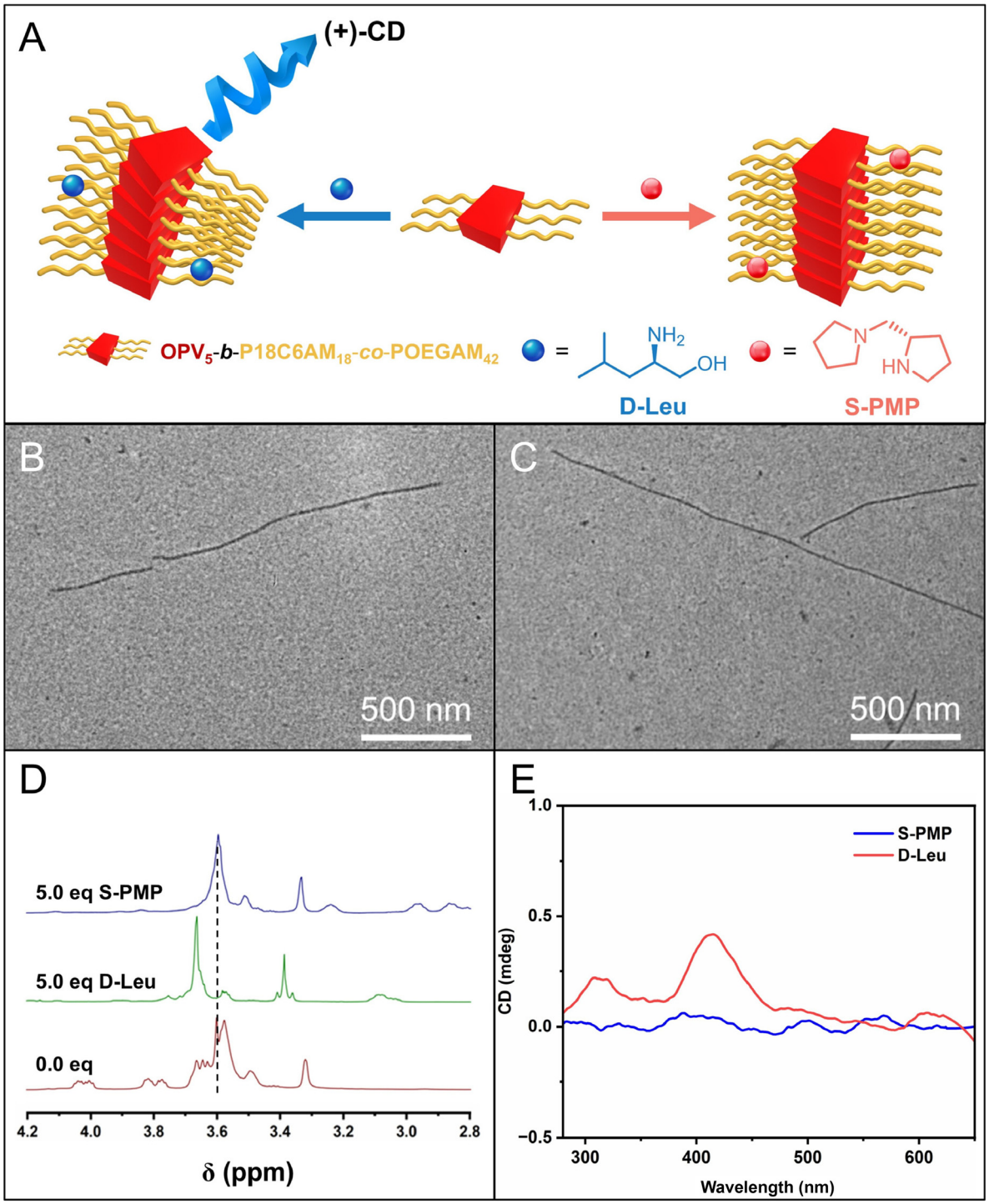

Fig. 5 (A) Schematic illustration of the co-assembly of OPV_5-*b*-$P18C6AM_{18}$-*co*-$POEGAM_{42}$ with *S*-PMP and *D*-Leu. TEM images of the fiber-like micelles of OPV_5-*b*-$P18C6AM_{18}$-*co*-$POEGAM_{42}$ formed with (B) *S*-PMP and (C) *D*-Leu, respectively. (D) ^1H NMR spectra of $P18C6AM_{18}$-*co*-$POEGAM_{42}$ without and with the addition of *S*-PMP and *D*-Leu. (E) CD spectra of micellar solutions of OPV_5-*b*-$P18C6AM_{18}$-*co*-$POEGAM_{42}$ formed with *S*-PMP and*D*-Leu.

Co-self-assembly of OPV_5-*b*-P18C6AM$_{18}$-*co*-POEGAM$_{42}$ with chiral amines. As previous results also demonstrated that 18C6 units can complex with amine units,[48,49] we then attempted to prepare helical fiber-like micelles of OPV_5-*b*-P18C6AM$_{18}$-*co*-POEGAM$_{42}$ using chiral amines of *D*-(−)-leucinol (*D*-Leu) and (*S*)-(+)-1-(2-pyrrolidinylmethyl)pyrrolidine (*S*-PMP) as inducing agents according to previous reports.[50,51] Aliquots of OPV_5-*b*-P18C6AM$_{18}$-*co*-POEGAM$_{42}$, which were taken from the same mother solution of OPV_5-*b*-P18C6AM$_{18}$-*co*-POEGAM$_{42}$, in the presence of *D*-Leu and *S*-PMP with a molar ratio of 18C6 to amines of 5 : 1, was subjected to the heating–cooling protocol. Firstly, TEM images showed that fiber-like micelles with a uniform width of 17.5 nm (Fig. 5B–C and S13†), comparable to those of fiber-like micelles without chiral amines, were still formed in the presence of *D*-Leu and *S*-PMP. The ^{1}H NMR spectra of P18C6AM$_{18}$-*co*-POEGAM$_{42}$ in the presence of *D*-Leu showed that the addition of *D*-Leu led to about a 0.14 ppm down-field shift of peaks attributed to the –OCH_2CH_2O– of 18C6 from 3.58 ppm to 3.72 ppm, while the presence of *S*-PMP only resulted in a 0.02 ppm down-field shift, which revealed much stronger complexation of 18C6 with *D*-Leu than *S*-PMP (Fig. 5D). These results illustrated that the complexation of 18C6 with *D*-Leu and *S*-PMP did not affect the formation of fiber-like micelles by CDSA of OPV_5-*b*-P18C6AM$_{18}$-*co*-POEGAM$_{42}$. More interestingly, circular dichroism (CD) analysis on the resulting micellar solution indicated that the micellar solution of OPV_5-*b*-P18C6AM$_{18}$-*co*-POEGAM$_{42}$ in the presence of *D*-Leu showed a predominantly positive Cotton effect with peaks at 417 nm attributed to the typical absorbance of OPV_5 segments, whereas the solution in the presence of *S*-PMP exhibited a very weak Cotton effect under the same conditions (Fig. 5E). All these results disclosed that the complexation of 18C6 with chiral amines can induce the helicity of the formed fiber-like micelles, which is an interesting topic deserving further investigation.

Synthesis and CDSA of OPV_5-*b*-PDMAEAM$_{66}$. To demonstrate the versatility of the PPFMA-based corona-forming precursor in the preparation of CPNFs by the combination of pentafluorophenyl ester chemistry and the self-seeding of living CDSA, the as-prepared azide-terminated PPFMA was treated with excess *N*,*N*-dimethylethyl-amine (Scheme 1). *In situ* ^{19}F NMR analysis on the reaction solution showed that the peaks at −150.64, −156.59 and −161.80 ppm attributed to the fluorine of the pentafluorophenyl units of PPFMA completely disappeared with the appearance of typical peaks at −167.58, −167.95 and −180.82 ppm that originated from pentafluorophenol (Fig. 6A). In the ^{1}H NMR spectrum of the purified product, a typical peak at 2.22 ppm attributed to the protons of the *N*,*N*-dimethylethyl moiety also appeared (Fig. S4†), indicative of the introduction of the *N*,*N*-dimethylethyl unit. Using the same protocol for the synthesis of OPV_5-*b*-P18C6AM$_{18}$-*co*-POEGAM$_{42}$, OPV_5-*b*-PDMAEAM$_{66}$ was prepared (details about its synthesis and characterization are provided in the ESI†). From the ^{1}H NMR spectrum of OPV_5-*b*-PDMAEAM$_{66}$, one can note typical peaks 'c' at 1.94 ppm and 'h'' at 4.06 ppm attributed to the –CH_2NCH_3– of PDMAEAM and the –OCH_2C$_5$H$_{11}$ of OPV_5 segments, respectively (Fig. 6B). From the integration ratio of peak "b" that originated from the protons of –CH_2CH_2N(CH_3)$_2$ of PDMAEAM to peaks "b′/c′/d′/e′/f′/g′" attributed to the protons of –Ar*H*– and –C*H*=C*H*– of OPV_5 segments, the number of DMAEAM repeat units was estimated to be about 66. GPC analysis also indicated a unimodal peak for the purified product of OPV_5-*b*-PDMAEAM$_{66}$ (Fig. S7†). All the above results ascertained the structure of OPV_5-*b*-PDMAEAM$_{66}$.

We then attempted to prepare fiber-like micelles of OPV_5-*b*-PDMAEAM$_{66}$ with an amino-containing (DMA-containing) corona by the heating–cooling protocol. The TEM image showed that the self-assembly of OPV_5-*b*-PDMAEAM$_{66}$, similar to OPV_5-*b*-P18C6AM$_{18}$-*co*-POEGAM$_{42}$, also gave fiber-like micelles with a uniform width of 15 nm and lengths up to several micrometers (Fig. 7B). The UV/vis absorption and FL fluorescence spectra of OPV_5-*b*-PDMAEAM$_{66}$ in THF almost overlapped with those of OPV_5-*b*-P18C6AM$_{18}$-*co*-POEGAM$_{42}$, which indicated that the

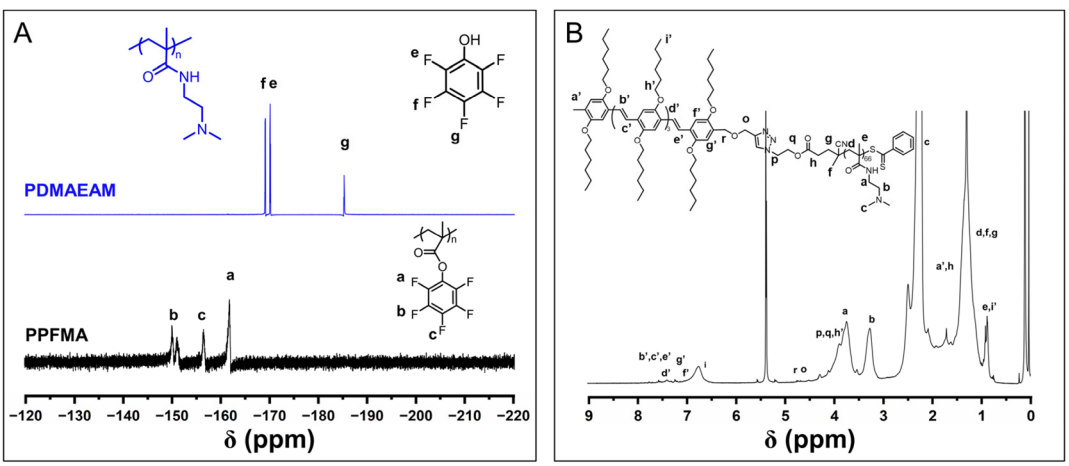

Fig. 6 (A) ^{19}F NMR spectra of azide-terminated PPFMA and the reaction solution for the preparation of PDMAEAM$_{66}$. (B) ^{1}H NMR spectrum of OPV_5-*b*-PDMAEAM$_{66}$ (CD_2Cl_2).

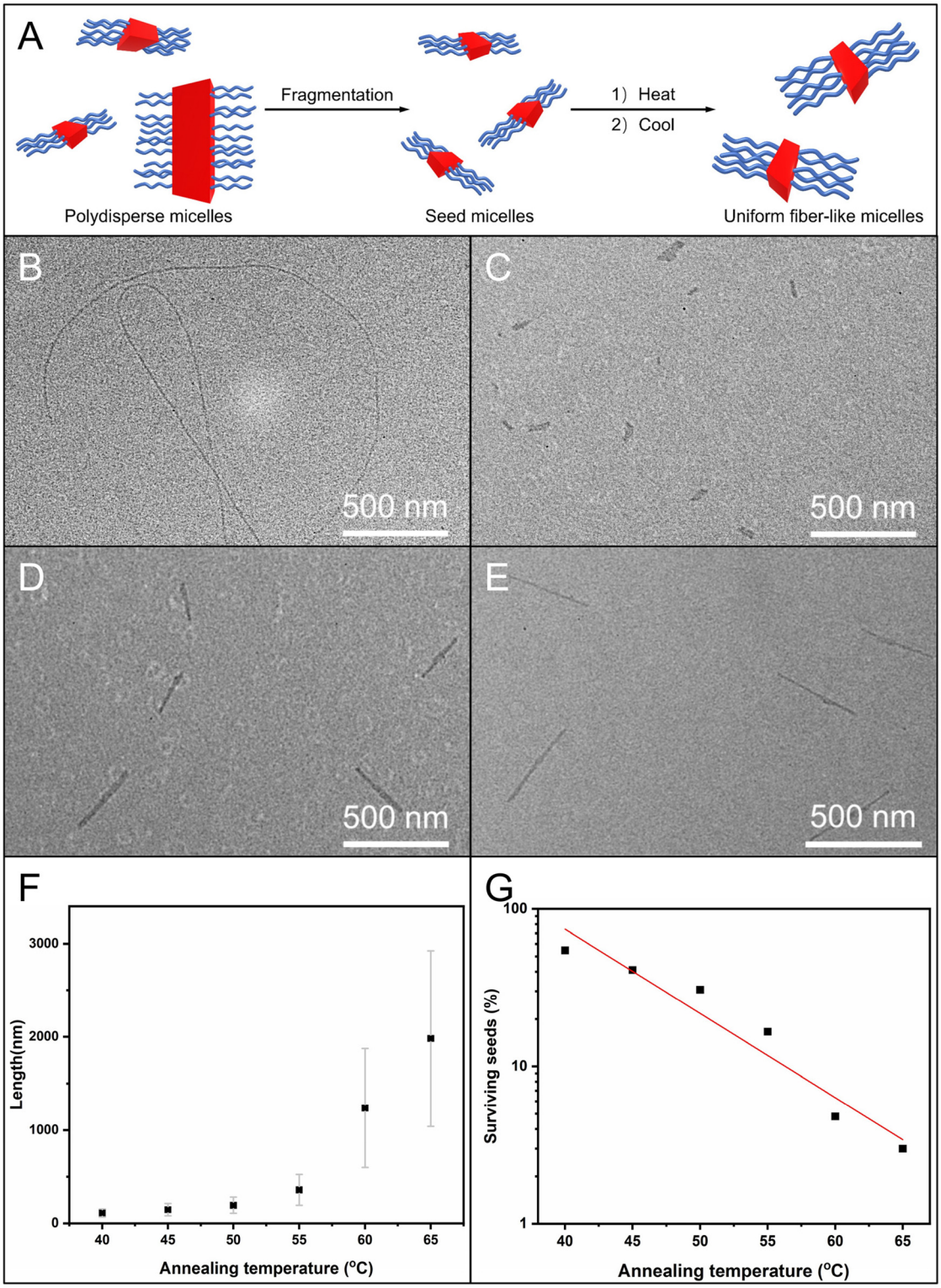

Fig. 7 (A) Schematic illustration of the preparation of uniform fiber-like micelles of OPV_5-*b*-$PDMAEAM_{66}$. Typical TEM images of (B) polydisperse, (C) seed and uniform fiber-like micelles of OPV_5-*b*-$PDMAEAM_{66}$ at annealing temperatures of (D) 50 °C and (E) 55 °C (0.05 mg mL^{-1} in ethanol). (F) L_n of fiber-like micelles and (G) semilogarithmic plot of the fraction of surviving seeds of OPV_5-*b*-$PDMAEAM_{66}$ *vs.* annealing temperature (0.05 mg mL^{-1} in ethanol).

change of corona-formation segments from P18C6AM$_{18}$-*co*-POEGAM$_{42}$ to PDMAEAM$_{66}$ did not affect the photophysical properties of OPV$_5$ in a unimolecularly dissolved state (Fig. S14†). Additionally, in comparison with the THF solution of OPV$_5$-*b*-PDMAEAM$_{66}$, the micellar solution of OPV$_5$-*b*-PDMAEAM$_{66}$ in ethanol also showed a blue-shift in the UV/vis absorption spectrum accompanied by a decrease in fluorescence intensity. These results also indicated that OPV$_5$ units adopt a single-layer H-aggregate mode to form the core of micelles.[29,37,45]

We further attempted to use the self-seeding approach for generating uniform fiber-like micelles of OPV$_5$-*b*-PDMAEAM$_{66}$ with tunable length (Fig. 7A). To this end, aliquots of seed micelles of OPV$_5$-*b*-PDMAEAM$_{66}$ (L_n = 60 nm, L_w/L_n = 1.29, 0.05 mg mL^{-1} in ethanol, Fig. 7C and Table S4†) were heated at temperatures from 40 °C to 65 °C, followed by cooling/aging at 25 °C for 24 h. TEM images showed that the L_n of the micelles increased from 109 nm to 194 nm with the increase in temperature from 40 °C to 50 °C and then abruptly increased from 359 nm to 1982 nm with the increase in temperature from 55 °C to 65 °C (Fig. 7D–E and S15, Table S4†). The fraction of surviving seeds also decreased exponentially with the temperature (Fig. 7G and Table S4†). All these results indicated that OPV$_5$-*b*-PDMAEAM$_{66}$ also demonstrated typical self-seeding behavior.[29,30]

Shell modification of fiber-like micelles of OPV$_5$-*b*-PDMAEAM$_{66}$. We then attempted to introduce extra functional moieties onto the surface of the resulting fiber-like micelles of OPV$_5$-*b*-PDMAEAM$_{66}$ by taking advantage of the dimethylamino (DMA) groups of the PDMAEAM corona, which were supposed to be able to serve as ligands to complex with metal ions and hydrogen-bonding acceptors. To demonstrate the formation of Ag NPs in the shell of micelles by utilizing PDMAEAM$_{66}$ as ligands, an aliquot of $AgPF_6$ in ethanol was added into the micellar solution of OPV$_5$-*b*-PDMAEAM$_{66}$ (0.05 mg mL^{-1} in ethanol), and the resulting mixture was allowed to age at 25 °C for 24 h (Fig. 8A). Subsequently, a reductant of $NaBH(CO_2CH_3)_3$ was added to reduce Ag^+ to Ag^0. As shown in Fig. 8B and S16,† dark dots with a diameter of ~9 nm appeared on the surface of ribbon-like micelles. Besides, owing to the hydrogen-bonding interaction of acidic moieties with the DMA groups of the PDMAEAM corona, an aliquot of metal clusters of phosphotungstic acid (0.026 mL, 1 mg mL^{-1} in water) used as a model acidic functional unit was added into the micellar solution of OPV$_5$-*b*-PDMAEAM$_{66}$ (0.05 mg mL^{-1} in ethanol, 0.1 mL) with a molar ratio of phosphotungstic acid to DMA of 0.33 and then the mixture was allowed to age at 25 °C for 24 h. From the TEM image of the resulting micelles with the addition of phosphotungstic acid

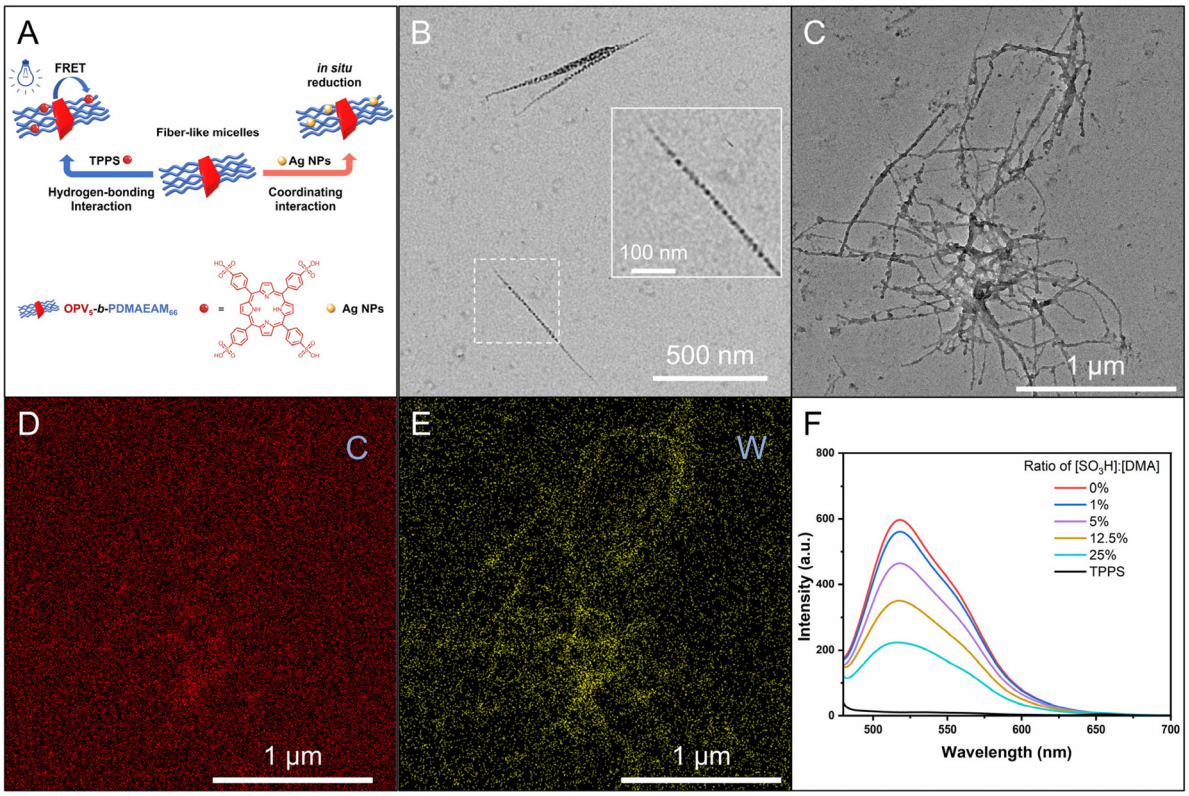

Fig. 8 (A) Schematic illustration of the surface functionalization of OPV-based CPNFs consisting of an OPV$_5$ core and a DMA-based corona with phosphotungstic acid and tetra-SO_3H-porphyrin moieties. TEM images of the fiber-like micelles of OPV$_5$-*b*-PDMAEAM$_{66}$ (B) coated with Ag NPs and (C) after the addition of phosphotungstic acid, respectively. STEM and elemental mapping of (D) C and (E) W of the fiber-like micelles of OPV$_5$-*b*-PDMAEAM$_{66}$ after the addition of phosphotungstic acid. (F) Fluorescence spectra of the micellar solution of OPV$_5$-*b*-PDMAEAM$_{66}$ after adding tetra-SO_3H-porphyrin moieties with varying molar ratios of [SO_3H] : [DMA].

(Fig. 8C), one can note fiber-shaped assemblies with a much rougher shell and larger width (17 to 40 nm) in comparison with pristine micelles before surface coating (Fig. 7B). Scanning transmission electron microscopy (STEM) with mapping C and W in energy-dispersive X-ray (EDX) spectroscopy analysis revealed that noticeable signals of W appeared and were consistent with the frame of fiber-like micelles (Fig. 8D and E). For further verification of interactions between acidic groups and DMA units and to demonstrate the versatility of DMA-based surface functionalization, different aliquots of tetra-SO_3H-porphyrin (0.01 mL, 3.86 mg mL^{-1} in DMSO) were added into the micellar solution of OPV_5-*b*-$PDMAEAM_{66}$ (0.05 mg mL^{-1} in ethanol, 0.3 mL) with molar ratios of $-SO_3H$ to DMA of 1%, 5%, 12.5% and 25%, respectively (Fig. 8A). The absorption and fluorescence spectra of tetra-SO_3H-porphyrin and the micellar solution of OPV_5-*b*-$PDMAEAM_{66}$ indicated favorable energy matching to allow the efficient Förster resonance energy transfer (FRET) from OPV_5 segments to tetra-SO_3H-porphyrin (Fig. 8F and S17†).[8,52,53] From the fluorescence spectra of the resulting mixtures, one can note that the fluorescence intensity at 518 nm originating from OPV_5 segments decreased with the increase in molar ratio, which showed the occurrence of FRET from OPV_5 segments to porphyrin units as indicated by the fluorescence quenching effect for OPV_5.[8] Since FRET only occurs when the distance between the energy donors and acceptors is below about 10 nm, the occurrence of FRET indicated the complexation of tetra-SO_3H-porphyrin to the PDMAEAM shell. All these results demonstrated that the acidic units, for example, phosphotungstic acid and tetra-SO_3H-porphyrin groups, can be immobilized onto the PDMAEAM shell of micelles by hydrogen-bonding interactions using the DMA units of PDMAEAM as hydrogen-bonding acceptors.

Conclusion

In summary, an azide-terminated PFMA was used as a versatile precursor to generate 18C6 and DMA-containing polymers that were subsequently coupled with alkyne-terminated OPV_5 to afford OPV_5-*b*-$P18C6AM_{18}$-*co*-$POEGAM_{42}$ and OPV_5-*b*-$PDMAEAM_{66}$, in which OPV_5 and 18C6/DMA-containing polymers were used as model π-conjugated segments and functional corona-forming blocks, respectively. Uniform fiber-like micelles with controlled length can be generated from both OPV_5-*b*-$P18C6AM_{18}$-*co*-$POEGAM_{42}$ and OPV_5-*b*-$PDMAEAM_{66}$. By taking advantage of the complexation capacity of 18C6 units, K^+ and Na^+ ions can be introduced into the corona. It was disclosed that the seed micelles of OPV_5-*b*-$P18C6AM_{18}$-*co*-$POEGAM_{42}$ upon complexation with K^+ and Na^+ ions showed much higher resistance toward dissolution. The 18C6 units can also complex with the chiral amines of *D*-Leu, which can induce the helicity of the resulting micelles to give a positive Cotton effect. In addition, by virtue of the coordinating ability and basicity of DMA units, AgNPs, metal clusters of phosphotungstic acid and SO_3H-containing porphyrins can be incorporated into the corona of the fiber-like micelles of OPV_5-*b*-$PDMAEAM_{66}$. Our results demonstrate that uniform CPNFs with varying shells can be efficiently prepared in a relatively facile and controlled way by the combination of pentafluorophenyl ester chemistry and the self-seeding of living CDSA. This work opens a facile and general platform for the generation of desired distinct CPNFs for diverse applications ranging from nanomedicine to (photo)catalysis.[54,55]

Author contributions

BX: investigation and formal analysis. CF and XYH: conceptualization, resources and funding acquisition. All authors reviewed and edited the manuscript.

Data availability

The data, including figures and tables, supporting this article have been included as part of the ESI.†

Conflicts of interest

The authors declare no competing financial interests.

Acknowledgements

The authors are thankful for financial support from the National Natural Science Foundation of China (52122314, U22A20131, 52173014 and 52361165657), the Strategic Priority Research Program of the Chinese Academy of Sciences (XDB0590000) and the Shanghai Scientific and Technological Innovation Project (22JC1401000 and 22ZR1475400). The authors thank Dr Kun Cui for his assistance with TEM measurements.

References

1 X. Li, P. J. Wolanin, L. R. MacFarlane, R. L. Harniman, J. Qian, O. Gould, T. G. Dane, J. Rudin, M. J. Cryan, T. Schmaltz, H. Frauenrath, M. A. Winnik, J. Faul and I. Manners, *Nat. Commun.*, 2017, **8**, 15909.
2 X. B. Lan, J. Chen, G. F. Liao and M. F. Zhu, *Adv. Fiber Mater.*, 2024, **6**, 943–945.
3 S. Ganda and M. H. Stenzel, *Prog. Polym. Sci.*, 2020, **101**, 101195.
4 J. Ma, G. Lu, X. Huang and C. Feng, *Chem. Commun.*, 2021, **57**, 13259–13274.
5 J. Ma, C. Ma, X. Huang, P. H. H. de Araujo, A. K. Goyal, G. Lu and C. Feng, *Fundam. Res.*, 2023, **3**, 93–101.
6 J. C. Foster, S. Varlas, B. Couturaud, Z. Coe and R. K. O'Reilly, *J. Am. Chem. Soc.*, 2019, **141**, 2742–2753.

7 C. Clamor, S. D. Dale, J. Beament, E. Mould, R. K. O'Reilly and A. P. Dove, *Macromolecules*, 2023, **56**, 9821–9828.
8 Y. Zhang, J. Tian, H. Shaikh, H. K. MacKenzie, Y. He, C. Zhao, S. Lei, Y. Ren and I. Manners, *J. Am. Chem. Soc.*, 2023, **145**, 22539–22547.
9 H. C. Parkin, J. D. Garcia-Hernandez, S. T. G. Street, R. Hof and I. Manners, *Polym. Chem.*, 2022, **13**, 2941–2949.
10 S. T. G. Street, Y. He, R. L. Harniman, J. D. Garcia-Hernandez and I. Manners, *Polym. Chem.*, 2022, **13**, 3009–3025.
11 S. Shin, F. Menk, Y. Kim, J. Lim, K. Char, R. Zentel and T. Choi, *J. Am. Chem. Soc.*, 2018, **140**, 6088–6094.
12 Y. Mai and A. Eisenberg, *Chem. Soc. Rev.*, 2012, **41**, 5969–5985.
13 W. Yu, J. C. Foster, A. P. Dove and R. K. O'Reilly, *Macromolecules*, 2020, **53**, 1514–1521.
14 J. Schmelz, M. Karg, T. Hellweg and H. Schmalz, *ACS Nano*, 2011, **5**, 9523–9534.
15 Z. Tong, Y. Xie, M. C. Arno, Y. Zhang, I. Manners, R. K. O'Reilly and A. P. Dove, *Nat. Chem.*, 2023, **15**, 824–831.
16 S. H. Hwang, S. Y. Kang, S. Yang, J. Lee and T. L. Choi, *J. Am. Chem. Soc.*, 2022, **144**, 5921–5929.
17 Y. W. Su, Y. K. Jiang, L. P. Liu, Y. J. Xie, S. C. Chen, Y. J. Wang, R. K. O'Reilly and Z. Z. Tong, *Macromolecules*, 2022, **55**, 1067–1076.
18 B. Jin, Q. Li, L. Hu, Q. Liu, Y. Chen, Y. Luo, S. Chi and X. Y. Li, *Angew. Chem., Int. Ed.*, 2023, e202219067.
19 B. Jin, K. Sano, S. Aya, Y. Ishida, N. Gianneschi, Y. Luo and X. Y. Li, *Nat. Commun.*, 2019, **10**, 2397.
20 C. Wang, L. Xu, L. Zhou, N. Liu and Z. Q. Wu, *Angew. Chem., Int. Ed.*, 2022, **61**, e202207028.
21 L. Xu, C. Wang, Y.-X. Li, X.-H. Xu, L. Zhou, N. Liu and Z. Q. Wu, *Angew. Chem., Int. Ed.*, 2020, **59**, 16675–16682.
22 N. K. Yun, C. Kang, S. H. Yang, S. H. Hwang, J. M. Park and T. L. Choi, *J. Am. Chem. Soc.*, 2023, **145**, 9029–9038.
23 X. Wang, G. Guerin, H. Wang, Y. Wang, I. Manners and M. A. Winnik, *Science*, 2007, **317**, 644–647.
24 X.-H. Jin, M. Price, J. R. Finnegan, C. E. Boott, J. Richter, A. Rao, S. Matthew Menke, R. H. Friend, G. R. Whittell and I. Manners, *Science*, 2018, **360**, 897–900.
25 S. K. Patra, R. Ahmed, G. R. Whittell, D. J. Lunn, E. L. Dunphy, M. A. Winnik and I. Manners, *J. Am. Chem. Soc.*, 2011, **133**, 8842–8845.
26 J. Qian, X. Li, D. J. Lunn, J. Gwyther, Z. M. Hudson, E. Kynaston, P. A. Rupar, M. A. Winnik and I. Manners, *J. Am. Chem. Soc.*, 2014, **136**, 4121–4124.
27 U. Tritschler, J. Gwyther, R. L. Harniman, G. R. Whittell, M. A. Winnik and I. Manners, *Macromolecules*, 2018, **51**, 5101–5113.
28 E. L. Kynaston, O. E. C. Gould, J. Gwyther, G. R. Whittell, M. A. Winnik and I. Manners, *Macromol. Chem. Phys.*, 2015, **216**, 685–695.
29 D. Tao, C. Feng, Y. Cui, X. Yang, I. Manners, M. A. Winnik and X. Huang, *J. Am. Chem. Soc.*, 2017, **139**, 7136–7139.
30 J. Nie, Z. Wang, X. Huang, G. Lu and C. Feng, *Macromolecules*, 2020, **53**, 6299–6313.
31 S. Yang and T. L. Choi, *Chem. Sci.*, 2020, **11**, 8416–8424.
32 J. Schmelz, A. Schedl, C. Steinlein, I. Manners and H. Schmalz, *J. Am. Chem. Soc.*, 2012, **134**, 14217–14225.
33 N. Petzetakis, A. P. Dove and R. K. O'Reilly, *Chem. Sci.*, 2011, **2**, 955–960.
34 M. C. Arno, M. Inam, Z. Coe, G. Cambridge, L. J. Macdougall, R. Keogh, A. P. Dove and R. K. O'Reilly, *J. Am. Chem. Soc.*, 2017, **139**, 16980–16985.
35 M. Wang, L. Han, Y. Zhu, R. Qi, L. Tian and F. He, *Small Methods*, 2019, **4**, 1900470.
36 X. Yang, J. Ruan, C. Ma, B. Hao, X. Huang, G. Lu and C. Feng, *Polym. Chem.*, 2019, **10**, 4718–4731.
37 D. Tao, C. Feng, Y. Lu, Y. Cui, X. Yang, I. Manners, M. A. Winnik and X. Huang, *Macromolecules*, 2018, **51**, 2065–2075.
38 D. Tao, Y. Cui, X. Huang, G. Lu, I. Manners, M. A. Winnik and C. Feng, *J. Colloid Interface Sci.*, 2020, **560**, 50–58.
39 J. Nie, L. Xia, X. Huang, G. Lu and C. Feng, *Polym. Chem.*, 2023, **14**, 2987–2997.
40 C. Duan, B. Xu, R. Li, X. Huang, S. Lin and C. Feng, *Sci. China: Chem.*, 2024, **67**, 2341–2352.
41 T. Gädt, F. H. Schacher, N. McGrath, M. A. Winnik and I. Manners, *Macromolecules*, 2011, **44**, 3777–3786.
42 M. Eberhardt, R. Mruk, R. Zentel and P. Théato, *Eur. Polym. J.*, 2005, **41**, 1569–1575.
43 A. Das and P. Theato, *Macromolecules*, 2015, **48**, 8695–8707.
44 Y. Que, Y. Liu, W. Tan, C. Feng, P. Shi, Y. Li and X. Huang, *ACS Macro Lett.*, 2016, **5**, 168–173.
45 Y. Song, B. Xiang, X. Y. Huang, G. L. Lu and C. Feng, *Chin. J. Polym. Sci.*, 2023, **41**, 574–584.
46 A. Jabbari and M. Shamsipur, *Spectrosc. Lett.*, 1993, **26**, 1715–1724.
47 R. M. Izatt, K. Pawlak, J. S. Bradshaw and R. L. Bruening, *Chem. Rev.*, 1991, **91**, 1721–2085.
48 V. Rüdiger, H. J. Schneider, V. P. Solov'ev, V. P. Kazachenko and O. A. Raevsky, *Eur. J. Org. Chem.*, 1999, 1847–1856.
49 R. Ji, C. G. Chao, Y. C. Huang, Y. Lan, C. L. Lu and T. Y. Luh, *Macromolecules*, 2010, **43**, 8813–8820.
50 R. Nonokawa, M. Oobo and E. Yashima, *Macromolecules*, 2003, **36**, 6599–6606.
51 R. Sakai, I. Otsuka, T. Satoh, R. Kakuchi, H. Kaga and T. Kakuchi, *Macromolecules*, 2006, **39**, 4032–4037.
52 Y. Wang, R. Zhu, Y. Hang, R. Wang, R. Dong, S. Yu and L. B. Xing, *Polym. Chem.*, 2023, **14**, 248–252.
53 H. Yang, S. Guo, B. Jin, Y. Luo and X. Y. Li, *Polym. Chem.*, 2022, **13**, 4887–4894.
54 C. Zhu, J. Wu, J. Yan and X. Liu, *Adv. Fiber Mater.*, 2023, **5**, 12–35.
55 X. Lv, Y. Liu, J. Yu, Z. Li and B. Ding, *Adv. Fiber Mater.*, 2023, **5**, 401–428.